Article Type | DOI:10.5281/zenodo.8007887
www.jnanosam.com

NANOSAM
Journal of NanoScience in Advanced Materials

Exploring Magnetic Properties through Structural Characterization of PtNi Alloy Nanoparticle

Mustafa Zeki Kurt[#]

The control of magnetic properties of ferromagnetic metals is an important objective in alloying with noble metals. In this study, the structural and magnetic properties of PtNi nanoparticle (NP) were investigated through the alloying of Ni with Pt. The $Pt_{0.5}Ni_{0.5}$ NP was synthesized using a modified polyol process. X-ray diffraction and Rietveld refinement analyses were conducted to determine the structural properties of the NP, revealing that they had an alloy form and an fcc-crystal structure with a space group of $Fm\bar{3}m$. The lattice constant and $d_{(111)}$-space of the PtNi NP were determined to be $a=b=c=0.38221$ nm and 2.2067 Å, respectively. Scanning electron microscope images and energy-dispersive X-ray spectra data confirmed that the NP was produced with high precision and without contamination; however, there was some degree of agglomeration. Magnetization curves were measured as a function of temperature between 5 K and 300 K, revealing three regions: paramagnetic between 200 K and 300 K, paramagnetic/ferromagnetic between 35 K and 200 K, and superparamagnetic/ferromagnetic regions below 35 K. Although no clear saturation magnetization region was observed up to ±3 T, the maximum magnetic moment of 4.26 emu/g was recorded at 5 K. This value decreased to 0.12 emu/g with increasing temperature to 300 K. Similarly, the coercive field was found to be 211 Oe at 5 K, and the hysteresis gap disappeared with increasing temperature, indicating a strong paramagnetic signal in the structure. The effective anisotropy constant was reduced to 3.01 $\times 10^6$ erg/cm^3, and the effective magnetic moment was reduced to 0.0937 μ_B due to the paramagnetic contribution of Pt in the alloy with Ni.

1. Introduction

Bimetallic alloy nanoparticles (NPs) have recently been recognized as promising materials for various technological applications, particularly for magnetic purposes. The incorporation of two or more metals into the NPs structure can lead to enhanced magnetic properties, such as increased remanence, saturation magnetization, and coercivity [1]. Moreover, bimetallic NPs can exhibit tunable magnetic behavior through controlled alloying of the constituent metals. This has attracted significant attention in the field of magnetic data storage, magnetic resonance imaging (MRI), and magnetic sensors [2-4]. In addition to their magnetic properties, bimetallic NPs also offer excellent chemical and thermal stability, making them suitable for harsh operating conditions. Therefore, extensive research has emerged on the synthesis and characterization of bimetallic alloy NPs, including PtFe, PtCo, PdFe, PdCo, and PtNi, among others, for various magnetic applications [5, 6]. Platinum-nickel (PtNi) nanoparticles have garnered attention in recent years for their potential in various technological applications, such as high-density data recording technologies, magnetoresistive sensors and biomedical applications, such as detection of bacteria, drug delivery, contrast agents, viruses, and proteins [7-9]. Binary metal alloy NPs, in particular, are extensively explored for their magnetic, electronic, optical and catalytic properties. Loading platinum-based NPs with ferromagnetic nickel atoms can enhance their chemical stability and catalytic activities, as well as allow control over their magnetic properties [10, 11]. Previous studies have shown that reducing the size and below the blocking temperature, T_B, of PtNi alloy NPs results in superparamagnetic, which further adds to their potential applications [10, 12]. While PtFe alloy NPs are widely used in permanent magnets and as magnetic bit [13-15], PtNi NPs provide promising properties for both magnetic and catalytic due to its high activity and chemical stability for hydrogen gas

Cukurova University, Faculty of Art and Sciences, Department of Physics, 01330, Adana, Türkiye
#Corresponding author: mzkurt@cu.edu.tr

Keywords: PtNi alloy, Polyol process, XRD, SEM-EDS, Magnetic properties

Received: 19 April 2023 | Accepted: 08 May 2023 | Published online: 25 June 2023

NANOSAM
Journal of NanoScience in Advanced Materials

production when compared to commercially available Pt/C.

PtNi bimetallic alloy NPs have been widely studied due to their promising applications in magnetoresistive sensor technologies, and magnetic resonance imaging, ultra-high density data recording, and catalysis [7, 8, 16]. To achieve the desired properties for these applications, it is crucial to control the structural properties (e.g. size, shape, crystal structure) of the nanoparticles. The polyol process has been identified as a promising method for producing PtNi NPs with high precision, small size, and without agglomeration. In this method, ethylene glycol and other 1,2-diols are used as reducing agents, while polyvinylpyrrolidone and other surface coating agents are employed to control the particle size and shape [17]. The addition of auxiliary reducing agents, such as hydrazine, sodium hypophosphite, or sodium borohydride, further reduces the particle size, leading to what is known as the modified polyol process. Experimental results have shown that sodium borohydride ($NaBH_4$) is a secondary reducing agent that can effectively decrease the crystalline size of PtNi NPs [18]. Overall, the polyol process offers a promising method for producing small, monodisperse PtNi NPs with controlled properties, making them suitable for a range of technological applications.

In this research, the magnetic properties of Ni were targeted for modification by introducing Pt into its structure, which was expected to decrease the magnetization levels of the samples. To achieve this, a modified polyol process was employed to synthesize PtNi alloy nanoparticle. Then, the crystal structure and the morphological analysis of PtNi alloy nanoparticles were determined with a comprehensive analysis, the magnetic properties of the NP was studied, including coercive field, blocking temperature, saturation magnetization, effective magnetic anisotropy constant, and effective magnetic moment.

2. Results and Discussion

2.1. Structural properties

The PtNi alloy NP were analyzed in detail by XRD and Rietveld refinement. The XRD pattern of the $Pt_{0.47}Ni_{0.53}$ NP is presented in Figure 1, which includes experimental data represented by red hollow circles, Rietveld refinement analysis by a black line, difference by a blue line, and Bragg positions shown by green bars. The measured and calculated values of 2θ degree, the miller indices, full width at half maximum (FWHM), *d*-spacing, crystallite size, and micro strain of the PtNi NP peaks were summarized in Table 1. As reported in Table 1, the miller indices of (111), (200), (220), and (311) planes were assigned to the reflection peaks of $Pt_{0.5}Ni_{0.5}$ NP at 2θ=41.0°, 48.2°, 68.8°, and 83.4°, respectively [8]. The lattice constant of the PtNi sample was found to be $a=b=c$=0.38221 nm for fcc-PtNi NP formation which is in between the lattice constant of pure-Pt, and Ni NPs were found to be 0.3953 nm [19] and 0.35214 nm [20] in earlier studies. The lattice constant increased due to the ionic radius of Pt atoms in the Ni alloy structure. When moving down a group in the periodic table, atoms gain an additional electron shell, resulting in an increase in the ionic radius of elements in that group. This explains why the lattice size of PtNi is greater than that of pure Ni crystals, as Ni atoms are replaced by Pt atoms. There were no other peaks observed indicating the formation of pure Pt and Ni crystal phases, which confirmed the complete formation of the PtNi alloy. The face-centered cubic (fcc) crystal structure with a space group of $Fm\bar{3}m$ was confirmed by Rietveld refinement analysis [7, 8]. The wide peak observed at around 2θ=23.5° corresponds to the glass substrate used during the measurement. The PtNi NP was successfully synthesized with an only PtNi crystal formation without the formation of oxides or by-products.

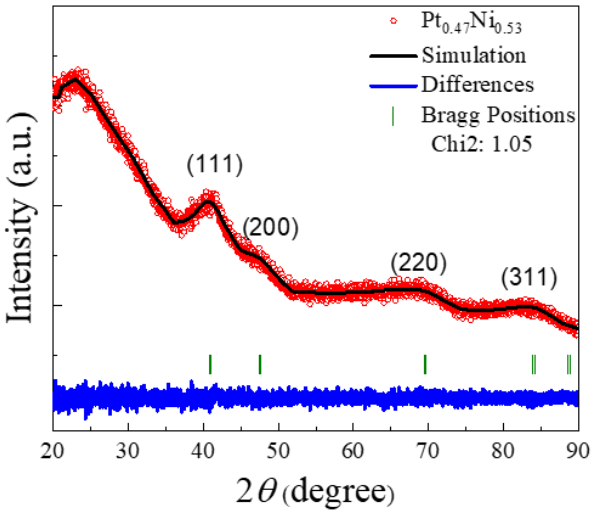

Figure 1. (a) XRD analysis of the $Pt_{0.47}Ni_{0.53}$ NP presented which comprises of experimental data shown by red hollow circles, Rietveld refinement analysis depicted by a black line, the difference shown by a blue line, and Bragg positions illustrated by green bars.

The FWHM values were determined fitting the experimental data by performing Rietveld Refinement analysis, and then *d*-spacing (Å), crystallite size (nm), and micro strain (%) were calculated and presented in Table 1. Here, the *d*-spaces were found to be 2.2067 Å, 1.9111 Å, 1.3513 Å, and 1.1524 Å corresponds to the (111), (200), (220), and (311) planes, respectively. The reduction

in d space for a given set of Miller indices (h, k, l) is due to the shape of the unit cell because the d spacing is a measure of the distance between adjacent crystal planes in the crystal lattice. The Miller indices indicate the orientation of the crystal planes, and the shape and size of the unit cell determine the distances between the planes. Similarly, the crystalline size was calculated using the Scherrer's Formula, $D_p=K\lambda/(B\ cos\theta)$ and were found to be 9.8 nm, 5 nm, 2.9 nm, and 3.8 nm for the (111), (200), (220), and (311) planes, respectively [21]. Here, D_p is the average crystallite size (nm), K is the Scherrer constant which is taken as 0.94 for spherical particles, λ is the X-ray wavelength which is taken as λ=1.54 Å, and B is the FWHM of XRD peak. The maximum micro Strain (%) value were recorded as 3.8917% for the (111) plane.

Figure 2 presents SEM images of $Pt_{0.47}Ni_{0.53}$ NP, where (a and c) and (b and d) are magnified at 400000X and 600000X, respectively. The images reveal that PVP-decorated NPs have a nearly spherical shape, and their distribution varies due to the presence of PVP molecules. Elemental analysis of the NP was conducted using EDS on a selected area in Figure 3(a). The results show typical atomic intensities of Pt and Ni atoms along with C and O background peaks arise from the carbon tape, and their respective electron shells. Despite the starting entry ratio being 50/50, EDS atomic percentages determined the stoichiometry of Pt and Ni in the PtNi nanoalloy compound to be 47% and 53%, respectively. The XRD and EDS analyses indicated that no impurity and other crystalline phases in structure.

2.2. Magnetic Properties

The magnetic properties of PtNi alloy NP were investigated under varying temperatures and applied magnetic fields. The magnetization-temperature, *M-T*, curve was obtained between 5 K and 300 K with applied fields of 250 Oe and 500 Oe, under both zero-field cooled (ZFC) and field cooled (FC) conditions (see Fig.4). The *M-T* curve exhibited three distinct regions: the first region was observed between 200 K and 300 K, where the magnetization was close to zero due to the paramagnetic contribution of Pt atoms. The second region occurred between 25 K and 200 K, where the magnetization increased linearly due to the lowering of the system energy and alignment of the magnetic spins with the direction of the applied field, resulting in a transition from paramagnetic to partial ferromagnetic behavior. The last region was observed at lower temperatures, where the PtNi NP exhibited two distinct behaviors, superparamagnetic and dominant ferromagnetic. The ZFC curve (solid square) measured with an applied field of 250 Oe displayed a peak at 35 K, which is known as the blocking temperature (T_B) [7]. Below this temperature, the PtNi NP exhibited superparamagnetic behavior with single domain spin alignments. This transition was not observed with an applied field of 500 Oe, and the partial ferromagnetic behavior became dominant. The effect of applied field results showed that T_B value disappeared by increasing the field from 250 Oe to 500 Oe due to less thermal energy required for the spin rotation of the particles [22]. The FC curves (hollow square and circle) for both applied fields exhibited similar behavior with a slightly higher magnetization at 500 Oe. The decrease in the applied field from 500 Oe to 250 Oe resulted in the appearance of a superparamagnetic signal due to the sufficient applied field. Similar behavior for PtNi NP also was observed in previous studies [7, 10].

Figure 5(a) shows the magnetization curves as a function of applied field (±3 T) at different temperatures, namely 5 K (black square), 50 K (red circle), and 300 K (blue triangle).The hysteresis loops exhibit temperature-dependent behavior, where the loops at 5 K show a higher magnetic moment compared to those at 50 K and 300 K. Moreover, the magnetic properties and hysteresis loops reduce at 300 K. The saturation magnetization, M_s, does not exhibit a distinct value at all temperatures, and the maximum value of M_s was found to be 4.26 emu/g, 1.37 emu/g, and 0.12 emu/g for the loop at 5 K, 50 K, and 300 K, respectively (see Table 2) [23]. The absence of saturation can be attributed to the strong paramagnetic signal from Pt and the applied field of ± 3 T, as well as the agglomeration of particles, which are not sufficient to align all magnetic spins in a multi-domain structure. Additionally, the coercive field, H_c, and the remanent magnetization M_r, , at all temperatures were analyzed, and their values were summarized in Table 2. A maximum hysteresis gap of 211 Oe was measured at 5K, where

Table 1. The summarized XRD data and Rietveld Refinement analysis results: 2θ degree, the miller indices, FWHM, *d*-spacing, crystallite size, and micro strain of the PtNi NP peaks.

°2θ	(h k l)	FWHM (°2θ)	*d*-spacing (Å)	Crystallite Size (nm)	Micro Strain (%)
40.9	(111)	3.514	2.2067	9.8	3.8917
47.6	(200)	9.006	1.9111	5	0.2993
69.6	(220)	6.432	1.3513	2.9	3.4033
84.0	(311)	6.911	1.1524	3.8	2.9753

NANOSAM
Journal of NanoScience in Advanced Materials

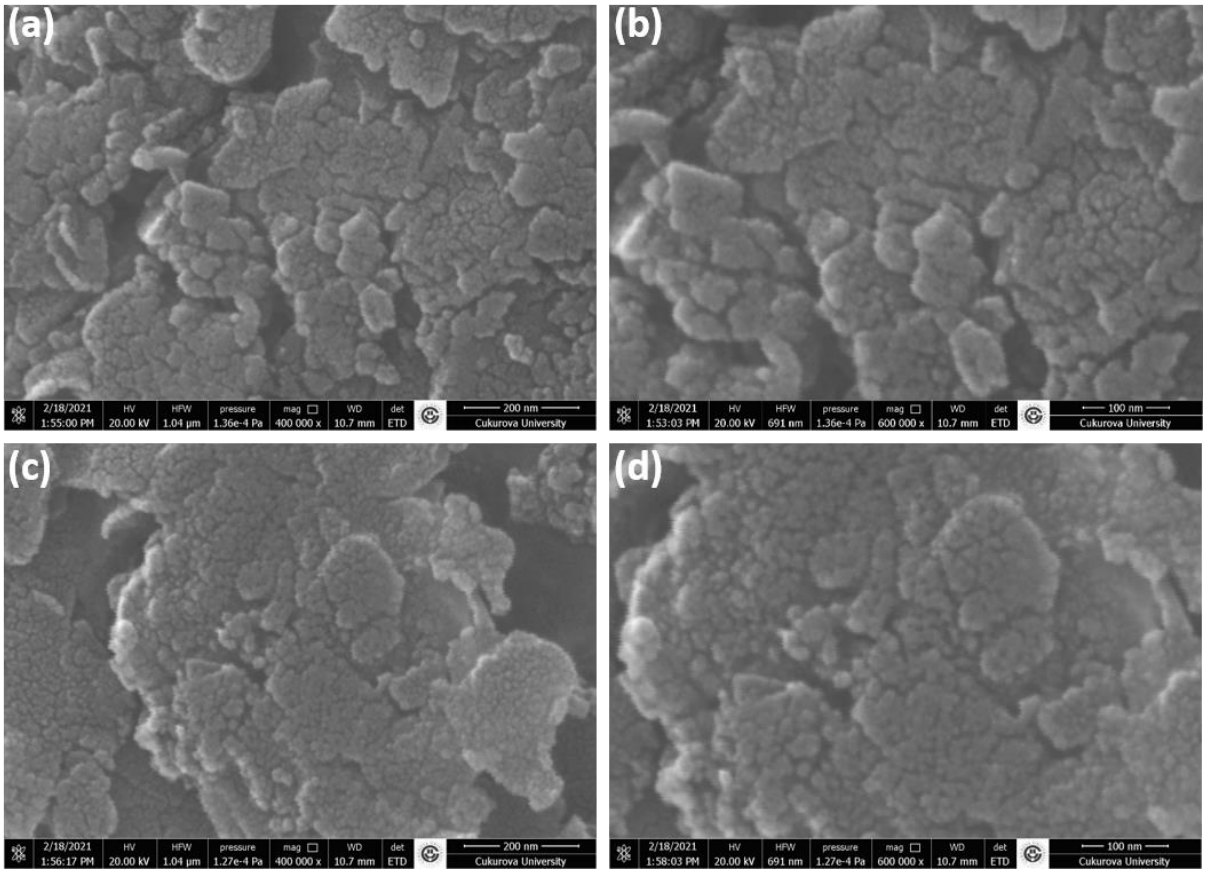

Figure 2. (a and c) The SEM images with a magnification of 400000X (b and d) with a magnification of 600000X were focused on a specific areas of the $Pt_{0.47}Ni_{0.53}$ NP.

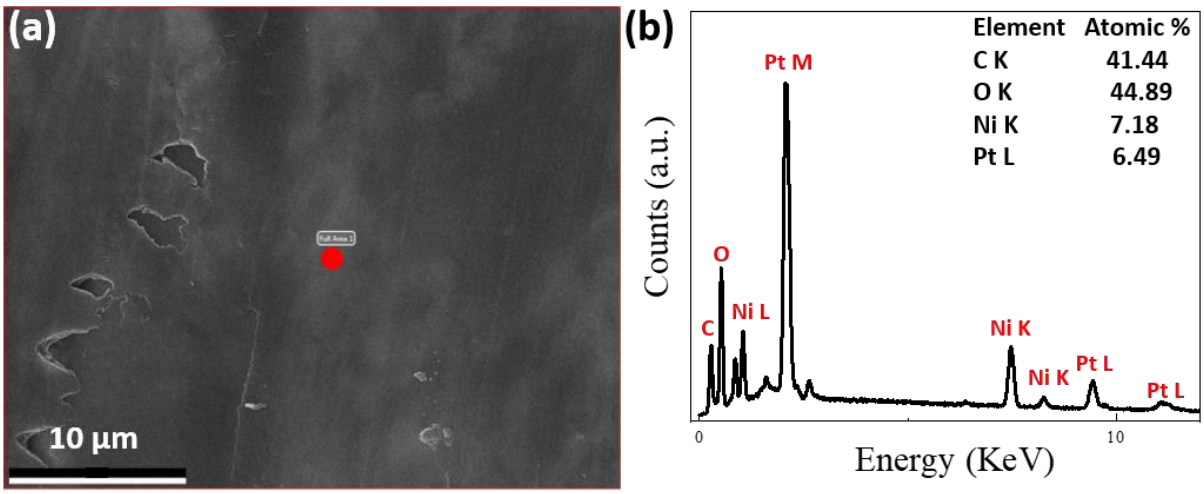

Figure 3. (a) The red market point was examined using a SEM and the resulting image was captured for the $Pt_{0.47}Ni_{0.53}$ NP. (b) The chemical composition of the sample was analyzed using EDS, which provided information about the elemental analysis and atomic intensities of Pt and Ni atoms along with background signals of C and O. An atomic percentage table was included as an inset to the EDS spectra.

NANOSAM
Journal of NanoScience in Advanced Materials

the ferromagnetic signal is dominant due to Ni [24]. However, the H_c values decreased with increasing temperature, first to 50 K and then to 300 K, in agreement with the *M-T* curves. Similarly, M_r values were recorded as 0.50 emu/g and 0.03 emu/g at 5 K and 50 K, respectively, while there is no M_r value was observed due to strong paramagnetic signal at 300 K (see Table 2) [25].

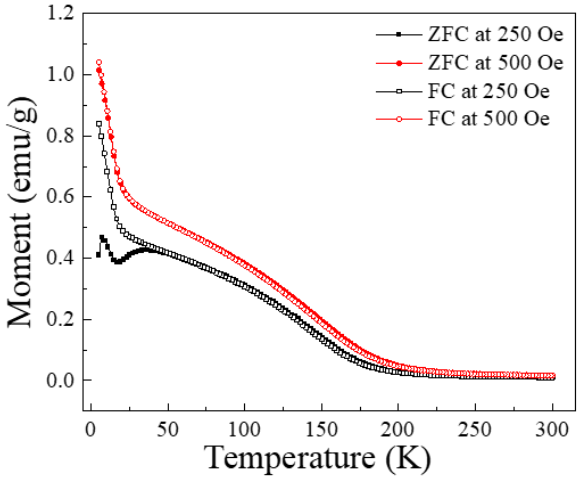

Figure 4. Magnetization curves of the $Pt_{0.47}Ni_{0.53}$ NP as a function of temperature between 5-300 K. ZFC (solid) and FC (hollow) curves recorded at 250 (black) and 500 Oe (red).

The superparamagnetic behavior of PtNi alloy nanoparticles was determined by calculating the effective anisotropy constant, K_{eff}, using the formula $K_{eff}=25*k_B*T_B/V$ [26]. Here, V is the particle volume in cm^3. The value of K_{eff} for $Pt_{0.47}Ni_{0.53}$ NP with T_B=35 K (see Table 2) was found to be 3.01×10^6 *erg/cm³*. Additionally, the effective magnetic moment, μ_{eff}, was calculated using $\mu_{eff}=(M_w\ M_s)/(N_A\ \beta)$ formula, where M_w is molecular weight of the materials, N_A is Avogadro number ($6.022\ 10^{23}$ mol^{-1}) and β is conversation factor (9.27×10^{-21} erg/Oe) [27]. The calculated values of μ_{eff} were 0.0937 μ_B, 0.0301 μ_B, and 0.0026 μ_B for 5 K, 50 K, and 300 K, respectively. These findings are comparable to earlier findings for Pt atoms, which was around 0.08 μ_B/atom [28].

Table 2. Summary of magnetic properties for all samples: blocking temperature (T_B), coercive field (H_c), saturation magnetization (M_s), and remanent magnetization (M_r), the effective magnetic moment (μ_{eff}), and the effective anisotropy constant, (K_{eff}) at 5 K, 50 K, and 300 K.

	Temperature (K)	$Pt_{0.47}Ni_{0.53}$ NP
T_B (K)		35
H_c (Oe)	5	211
M_S (emu/g)	5	4.26
	50	1.37
	300	0.12
M_r (emu/g)	5	0.50
	50	0.03
μ_{eff} (μ_B)	5	0.0937
	50	0.0301
	300	0.0026
K_{eff} (erg/cm³ 10^6)		3.01

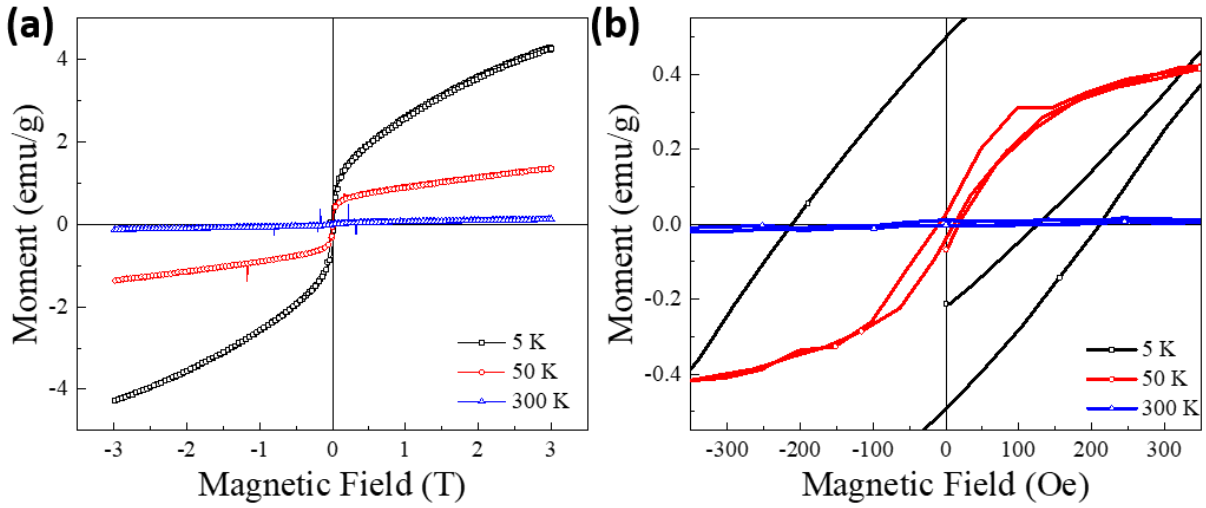

Figure 5. (a) Magnetization curves of the $Pt_{0.47}Ni_{0.53}$ NP as a function of applied magnetic field up to ±3 T measured at 5, 50, and 300 K. (b) Enlarged curve to show the points where it intersects the axes of the $Pt_{0.47}Ni_{0.53}$ NP.

3. Conclusion

Alloying ferromagnetic metals with noble metals is an important way to control their magnetic properties. The structural and magnetic properties of $Pt_{0.47}Ni_{0.53}$ NP was determined using X-ray diffraction and Rietveld refinement analyses, which revealed that fcc-crystal structure of PtNi NP with alloy form and with a space group of $Fm\bar{3}m$. The lattice constant and $d_{(111)}$-space of the PtNi NP were found to be a=b=c=0.38221 nm and 2.2067 Å, respectively. The images from the SEM and EDS data confirmed that the NP were produced precisely and without contamination. The magnetization curves were measured as a function of temperature between 5 K and 300 K, and three regions were observed: paramagnetic between 200 K and 300 K, paramagnetic/ferromagnetic between 35 K and 200 K, and superparamagnetic/ferromagnetic regions below 35 K. Although no clear saturation magnetization region was observed up to ±3 T, the maximum magnetic moment of 4.26 emu/g was recorded at 5 K. This value decreased to 0.12 emu/g with increasing temperature to 300 K. The coercive field was found to be 211 Oe at 5 K, and the hysteresis gap disappeared with increasing temperature, indicating a strong paramagnetic signal in the structure. Due to the paramagnetic contribution of Pt in the alloy with Ni, the effective anisotropy constant was reduced to 3.01 $\times 10^6$ erg/cm^3, and the effective magnetic moment was reduced to 0.0937 μ_B.

Method

Chemicals

Several metal precursors were utilized For the experiment, including Pt(II) acetylacetonate ($Pt(C_5H_7O_2)_2$, Sigma-Aldrich ≥97%) and Ni(II) acetylacetonate ($Ni(C_5H_7O_2)_2$, Sigma-Aldrich ≥95%). Ethylene glycol (EG-$(CH_2OH)_2$, Sigma-Aldrich ≥99.8%) and $NaBH_4$ (Sigma-Aldrich ≥98%), are initial and secondary reducing agent, respectively. To maintain the pH level around 9.5-10 in the mixture, sodium hydroxide (NaOH, Merck ≥99.8%) was added, while polyvinylpyrrolidone (PVP, Mav 40000) was utilized as a surfactant to prevent oxidation and agglomeration. N,N-Dimethylformamide (DMF-C_3H_7NO, Sigma-Aldrich ≥99.8%) was used for dissolving the precursors. The final product was washed using ethanol (ISOLAB, extra pure).

Synthesis of $Pt_{0.46}Ni_{0.54}$ NPs

In order to produce $Pt_{0.5}Ni_{0.5}$ NP, a three-necked flask was used to dissolve 0.788 mmol Pt (0.3099 g) and 0.788 mmol Ni (0.2024 g) precursors in 15 mL DMF. This solution was mixed with 50 mL EG, resulting in a light green color. After being refluxed for 30 minutes at 30°C, the mixture was combined with 3.152 mmol PVP (0.1261 g) and 23.643 mmol NaOH (0.9457 g) while under vigorous magnetic stirring and high-purity Ar gas flow. $NaBH_4$ (37.829 mmol, 1.4310 g) was then slowly added at 10 ml/min via a dropping funnel at 120 °C, causing the mixture color to turn black, indicating the formation of PtNi alloy NP. The mixture was refluxed for 60 minutes at 170 °C, then cooled to room temperature under Ar gas flow. The PtNi alloy NP were isolated from the by-products using ethanol washing and centrifugation at 9000 rpm for six minutes.

Characterization

Initially, the PtNi alloy NP structural characteristics were investigated through the utilization of a PANalytical EMPYREAN x-ray diffraction (XRD) system. This instrument operates under Bragg-Brentano geometry with Cu-$K\alpha$ radiation (λ=1.54 Å) and Rietveld refinement analysis was performed using Fullprof Software. The morphology and chemical composition of the NP was studied via FEI Quanta 650 scanning electron microscope (SEM) images and energy-dispersive x-ray spectra (EDS) data, respectively. The magnetization of the NP was measured with Quantum Design DynaCool-9 physical property measurement system using a vibrating sample magnetometer. The measurements were carried out with an applied field of 250 Oe and 500 Oe, between 5 and 300 K for the magnetization as a function of temperature, *M-T*, and between ±3 T at different temperatures for the magnetization as a function of an applied magnetic field, *M-H*.

Acknowledgements

The author gratefully acknowledges the valuable discussions and contributions to this work by Prof. Dr. Faruk Karadag and Prof. Dr. Ahmet Ekicibil.

Authors' contributions:

MZK performed all data curation, analysis, and writing paper.

Data Availability Statement

The data that support the findings of this study are available from the corresponding author upon reasonable request.

NANOSAM
Journal of NanoScience in Advanced Materials

References

[1] Kolhatkar, A., Jamison, A., Litvinov, D., Willson, R., and Lee, T. "Tuning the Magnetic Properties of Nanoparticles", International journal of molecular sciences **14** 15977-6009 (2013).

[2] Valdés, D.P., Torres, T.E., Moreno Maldonado, A.C., Urretavizcaya, G., Nadal, M.S., Vasquez Mansilla, M., Zysler, R.D., Goya, G.F., De Biasi, E., and Lima, E. "Thermographical Method to Assess the Performance of Magnetic Nanoparticles in Hyperthermia Experiments through Spatiotemporal Temperature Profiles", Physical Review Applied **19** (1) 014042 (2023).

[3] Sarveena, Shrivastava, N., Singh, M., and Sharma, S.K., *Multifunctional Magnetic Nanostructures: Exchange Bias Model and Applications*, in *Complex Magnetic Nanostructures: Synthesis, Assembly and Applications*, S.K. Sharma, Editor Springer International Publishing: Cham. p. 225-280 (2017)

[4] Litvinov, D., E, C., Parekh, V., Smith, D., Rantschler, J., Zhang, S., Donner, W., Lee, T.R., Ruchhoeft, P., Weller, D., and Khizroev, S. "Design and Fabrication of High Anisotropy Nanoscale Bit-Patterned Magnetic Recording Medium for Data Storage Applications", ECS Transactions **3** (25) 249-258 (2019).

[5] Abdelsayed, V., Glaspell, G., Nguyen, M., Howe, J.M., and Samy El-Shall, M. "Laser synthesis of bimetallic nanoalloys in the vapor and liquid phases and the magnetic properties of PdM and PtM nanoparticles (M = Fe, Co and Ni)", Faraday Discussions **138** (0) 163-180 (2008).

[6] Liu, Y., Li, D., and Sun, S. "Pt-based composite nanoparticles for magnetic, catalytic, and biomedical applications", Journal of Materials Chemistry **21** (34) 12579-12587 (2011).

[7] Du, J.-J., Yang, Y., Zhang, R.-H., and Zhou, X.-W. "Synthesis, characterization and magnetic properties of highly monodispersed PtNi nanoparticles", Materials Chemistry and Physics **155** 47-51 (2015).

[8] Huízar-Félix, A.M., Cruz-Silva, R., Barandiarán, J.M., García-Gutiérrez, D.I., Orue, I., Merida, D., and Sepúlveda-Guzmán, S. "Magnetic properties of thermally reduced graphene oxide decorated with PtNi nanoparticles", Journal of Alloys and Compounds **678** 541-548 (2016).

[9] Mathe, N.R., Nkosi, S.S., Motaung, D.E., Scriba, M.R., and Coville, N.J. "The Effect of Reducing Agents on the Electronic, Magnetic and Electrocatalytic Properties of Thiol-Capped Pt/Co and Pt/Ni Nanoparticles", Electrocatalysis **6** (3) 274-285 (2015).

[10] Kaya, D. "Synthesis and structural characterization of binary PtNi alloy nanoparticles: investigating magnetic transition", Journal of Materials Science: Materials in Electronics **32** (23) 27975-27986 (2021).

[11] Piotrowski, M.J., Piquini, P., and Da Silva, J.L. "Platinum-Based Nanoalloys Pt n TM55–n (TM= Co, Rh, Au): A Density Functional Theory Investigation", The Journal of Physical Chemistry C **116** (34) 18432-18439 (2012).

[12] Sun, X., Gutierrez, A., Yacaman, M.J., Dong, X., and Jin, S. "Investigations on magnetic properties and structure for carbon encapsulated nanoparticles of Fe, Co, Ni", Materials Science and Engineering: A **286** (1) 157-160 (2000).

[13] He, Y., Wu, Y.L., Zhu, X.X., and Wang, J.N. "Remarkable Improvement of the Catalytic Performance of PtFe Nanoparticles by Structural Ordering and Doping", ACS Applied Materials & Interfaces **11** (12) 11527-11536 (2019).

[14] Castellanos-Rubio, I., Insausti, M., de Muro, I.G., Arias-Duque, D.C., Hernández-Garrido, J.C., Rojo, T., and Lezama, L. "The impact of the chemical synthesis on the magnetic properties of intermetallic PdFe nanoparticles", Journal of Nanoparticle Research **17** (5) 229 (2015).

[15] Maenosono, S., Suzuki, T., and Saita, S. "Superparamagnetic FePt nanoparticles as excellent MRI contrast agents", Journal of Magnetism and Magnetic Materials **320** (9) L79-L83 (2008).

[16] Wu, D., Zhang, W., Lin, A., and Cheng, D. "Low Pt-Content Ternary PtNiCu Nanoparticles with Hollow Interiors and Accessible Surfaces as Enhanced Multifunctional Electrocatalysts", ACS Applied Materials & Interfaces **12** (8) 9600-9608 (2020).

[17] Fiévet, F., Ammar-Merah, S., Brayner, R., Chau, F., Giraud, M., Mammeri, F., Peron, J., Piquemal, J.Y., Sicard, L., and Viau, G. "The polyol process: a unique method for easy access to metal nanoparticles with tailored sizes, shapes and compositions", Chemical Society Reviews **47** (14) 5187-5233 (2018).

[18] Antolini, E., Salgado, J.R.C., da Silva, R.M., and Gonzalez, E.R. "Preparation of carbon supported binary Pt–M alloy catalysts (M=first row transition metals) by low/medium temperature methods", Materials Chemistry and Physics **101** (2) 395-403 (2007).

[19] Jeon, T.-Y., Lee, H.-K., Yoon, G.-H., Lee, S.-H., Yun, H.J., Kim, K.-J., Lee, K.-S., Pinna, N., and Yu, S.-H. "Selective dealloying of chemically disordered Pt–Ni bimetallic nanoparticles for the oxygen reduction reaction", Nanoscale **15** (3) 1136-1144 (2023).

[20] Moulana Kareem, M., Hari Babu, M., and Vijaya Lakshmi, G. "Anticancer, antibacterial, antioxidant, and photo-catalytic activities of eco-friendly synthesized Ni nanoparticles", Inorganic Chemistry Communications **148** 110274 (2023).

[21] Holzwarth, U. and Gibson, N. "The Scherrer equation versus the 'Debye-Scherrer equation'", Nature Nanotechnology **6** (9) 534-534 (2011).

[22] Suzuki, Y. and Miwa, S. "Magnetic anisotropy of ferromagnetic metals in low-symmetry systems", Physics Letters A **383** (11) 1203-1206 (2019).

[23] Liu, R., Zhao, Q., Li, Y., Zhang, G., Zhang, F., and Fan, X. "Graphene Supported Pt/Ni Nanoparticles as Magnetically Separable Nanocatalysts", Journal of Nanomaterials **2013** 602602 (2013).

[24] Sahoo, P.K., Panigrahy, B., and Bahadur, D. "Facile synthesis of reduced graphene oxide/Pt–Ni nanocatalysts: their magnetic and catalytic properties", RSC Advances **4** (89) 48563-48571 (2014).

[25] Sahoo, P.K., Panigrahy, B., Li, D., and Bahadur, D. "Magnetic behavior of reduced graphene oxide/metal nanocomposites", **113** (17) 17B525 (2013).

[26] Binns, C., *Chapter 1 - Tutorial Section on Nanomagnetism*, in *Frontiers of Nanoscience*, C. Binns, Editor Elsevier. p. 1-32 (2014)

[27] Kaya, D., Adanur, I., Akyol, M., Karadag, F., and Ekicibil, A. "Detailed investigation of structural and magnetic properties of multiphase binary Pd-Co alloys prepared by modified polyol process", Journal of Alloys and Compounds **876** 160157 (2021).

[28] Bezerra-Neto, M.M., Ribeiro, M.S., Sanyal, B., Bergman, A., Muniz, R.B., Eriksson, O., and Klautau, A.B. "Complex magnetic structure of clusters and chains of Ni and Fe on Pt(111)", Scientific Reports **3** (1) 3054 (2013).